Threshold of Shear-mode Fatigue Crack Growth in Bearing Steel

Hisao Matsunaga[1, a], Satoshi Muramoto[2, b] and Masahiro Endo[3, c]

[1, 3] Department of Mechanical Engineering, Fukuoka University,
8-19-1 Nanakuma, Jonan-ku, Fukuoka, 814-0180, Japan

[2] Graduate School of Fukuoka University

[a] hm@fukuoka-u.ac.jp, [b] td070011@fukuoka-u.ac.jp, [c] endo@fukuoka-u.ac.jp

Keywords: Shear-mode fatigue cracks, Small cracks, Torsional fatigue test under static compressive stress, Bearing steel, ΔK_{IIth}, $\Delta K_{\mathrm{IIIth}}$

Abstract. Semi-elliptical shear-mode fatigue cracks were studied in SAE52100 bearing steel loaded with fully-reversed cyclic torsion combined with a static axial compressive stress. Non-propagating cracks smaller than 1 mm in length were obtained in the following two ways; (i) decreasing stress amplitude tests using notched specimens, and (ii) constant stress amplitude tests using smooth specimens. The shape and dimensions of the non-propagating cracks were investigated by a successive polishing of the specimen surface, and the threshold stress intensity factor ranges, ΔK_{IIth} and $\Delta K_{\mathrm{IIIth}}$, were estimated. The threshold values decreased with a decrease in crack size. There was no significant difference between ΔK_{IIth} and $\Delta K_{\mathrm{IIIth}}$. Wear on the crack surfaces during crack-growth was inferred by a change in microstructure.

Introduction

Rolling-contact fatigue failures, such as flaking-type failure in bearings and shelling-type failure in railroad rails, are intimately related to shear-mode (modes II and III) fatigue crack-growth [1, 2]. In order to evaluate the fatigue strength quantitatively based on fracture mechanics, the behaviour of shear-mode crack-growth and threshold must be determined. However, they have been well understood neither qualitatively nor from a quantitative fracture mechanics point of view, though there have been some significant progresses in recent years. For example, with respect to the mode II threshold stress intensity factor range for bearing steel SAE52100, Otsuka *et al.* [3] made use of a decreasing, fully-reversed mode II testing method which prevented contact of the opposing crack faces. They found the mode II threshold to be approximately 3 $\mathrm{MPa \cdot m^{1/2}}$. In contrast, Murakami *et al.* [4] found in a decreasing ΔK_{II} test that when the opposing crack faces were allowed to contact and if the friction coefficient was hypothesized to be 1.0, ΔK_{IIth} was 13 ~ 15 $\mathrm{MPa \cdot m^{1/2}}$. There is a large discrepancy between these data but the cause has yet to be clarified. The following factors should be further elucidated; (i) small crack effect on shear-mode crack-growth, (ii) friction coefficient between crack-faces, (iii) mechanism of the microstructural changes, e.g. the "white microstructure" and the "butterfly" [5], and their role on the fatigue process, and (iv) the crack initiation mechanism (opening-mode or shear-mode), etc.

In the present study, semi-elliptical shear-mode fatigue cracks less than 1 mm in size were studied in cylindrical specimens of SAE52100 bearing steel. Cracks grew parallel to the specimen axis. The threshold stress intensity factor ranges, ΔK_{IIth} and $\Delta K_{\mathrm{IIIth}}$, were obtained from the shape and dimensions of the non-propagating cracks. Microstructural changes due to shear-mode crack-growth were also examined.

Experimental

Material. The studies were carried out on a commercial grade SAE52100 bearing steel. The chemical composition in wt. % was 0.98 C, 0.16 Si, 0.38 Mn, 0.12 P, 0.06 S, 0.12 Cu, 0.07 Ni, 1.39 Cr,

0.02 Mo and bal. Fe. The steel was heat-treated at 840°C for 30 minutes in a deoxiding gas followed by oil-quenching and tempered at 170°C for 2 hours. The average Vickers hardness *HV* measured with a load of 9.8 N was 753.

Specimen. Figure 1 shows the shape and dimensions of the specimen. The specimen surfaces were finished by polishing with an emery paper and then buffing with an alumina paste. In some specimens, three adjacent drill holes aligned with the specimen axis were introduced. Figure 2 shows the shape and dimensions of the holes. They have crack-like thin slits made by the focused ion beam (FIB) technique at the both ends to facilitate crack initiation. Total length of the defects ranged 240 ~ 440 μm and their depth ranged 80 ~ 200 μm. In the following, these defects are termed defect A and B, respectively.

Fatigue test. Cyclic torsion tests were carried out using a biaxial servo-hydraulic fatigue testing machine with a test frequency of 14 ~ 28 Hz and a stress ratio R of −1. To further reduce any tendency for mode I crack branching, an axial static compressive stress σ_m of −1200 or −1000 MPa was superposed on the torsional cyclic loading. The tests were periodically halted for microscopic observation of initiation and crack-growth.

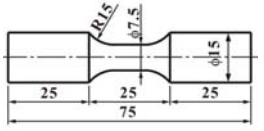

Figure 1 Shape and dimensions of fatigue test specimen (in mm)

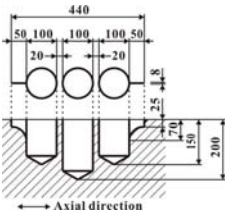

(a) Defect A

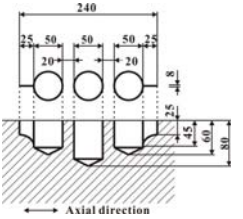

(b) Defect B

Figure 2 Shape and dimensions of holes having crack-like thin slits at the both ends (in μm)

Results and Discussion

Crack-growth in axial direction and non-propagating cracks. All the fatigue tests were started at a τ_a of 500 ~ 600 MPa, where τ_a is the shear stress amplitude at specimen surface. In the specimens having either defect A or B, shear-mode cracks were initiated from the crack-like slits and propagated in the axial direction.

Figure 3 shows a crack propagating from the defect A at τ_a of 600 MPa. Figure 4 shows the growth curve of shear-mode crack. In this case, the crack-growth rate was increased with an increase in crack length. Mode I crack branching was intermittently occurred at shear-mode crack tip. Lengths of the Mode I cracks were increased with the total length of shear-mode crack $2a$, and finally the fracture was dominated by mode I.

In order to suppress the mode I cracking and to determine threshold conditions for shear-mode crack-growth, τ_a was gradually decreased by 10 ~ 40 MPa with every increment in crack length $2a$ of 10 ~ 30 μm. In this case, little mode I crack branching, if any, was observed. When the crack stopped propagating at a shear stress amplitude for 10^7 cycles the test was finished and the crack was defined as a non-propagating crack. Figure 5 shows the growth curves of the cracks from defects A and B in the τ_a -decreasing tests. The crack-growth rate, da/dN, was less than 1×10^{-11} m/cycle in all the stress levels, the extremely slow growth rate subsequently became even slower just before the complete arrest. An abrasion powder continued to be observed due to wear of the crack-faces even after the cracks stopped propagating. Figures 6 (a) and (b) show optical micrographs of the non-propagating cracks. Figure 7 shows an example of abrasion powder occurring at crack faces.

Smooth specimens without artificial defects were also tested at a constant stress amplitude τ_a of 600 MPa. A number of cracks were initiated from MnS type inclusions which are elongated in the axial

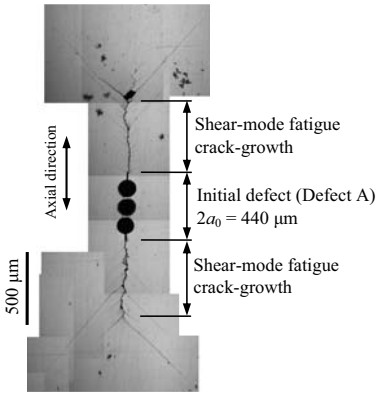

Figure 3 Crack-growth in axial direction and mode I crack branching (τ_a =600 MPa, σ_m = –1200MPa, $N = 9\times10^6$)

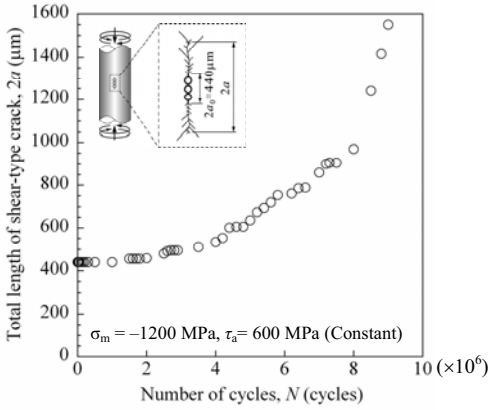

Figure 4 Crack-growth curve in τ_a -constant test (Defect A, τ_a =600 MPa, σ_m = –1200MPa)

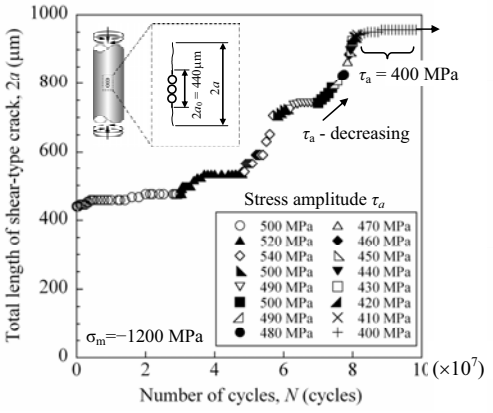

(a) Crack-growth from defect A

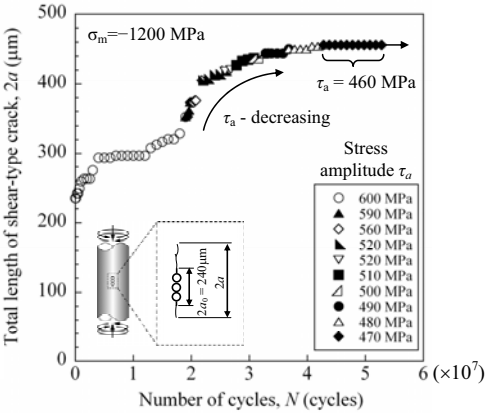

(b) Crack-growth from defect B

Figure 5 Crack-growth curves in τ_a -decreasing tests

direction. Most of the cracks became a non-propagating crack before 10^7 cycles without decreasing the stress amplitude, whereas a few cracks continued to propagate. Figures 6 (c) and (d) show examples of the non-propagating cracks in the smooth specimens.

Threshold of shear-mode crack-growth. Figure 8 shows the shape and dimensions of the non-propagating cracks shown in Fig. 6 which were obtained by a successive polishing. Amount of the thickness of polished layer was measured by the depth of drill holes which were introduced in the vicinity of the crack.

Threshold stress intensity factor ranges, ΔK_{IIth} and ΔK_{IIIth}, were estimated from these results. In a shear-mode semi-elliptical crack such as the cracks in Fig. 8, the propagating mode is mode III at the crack bottom. On the other hand, the propagation is mainly dominated in a mode II fashion in the vicinity of free surface. However, it is known that the nature of the crack tip singularity changes in the vicinity of a corner point where a crack front intersects a free surface [6-8]. It has also been pointed out that the crack front edge of a propagating crack should terminate at the surface obliquely [8]. For

these cases the stress intensity factor cannot be easily determined in the vicinity of the corner point. Therefore, in this study, stress intensity factor ranges, ΔK_{II} and ΔK_{III}, were estimated with Kassir and Sih's solution for an elliptical crack in an infinite body under uniform shear [9]. Poisson's ratio of the material was assumed to be 0.3.

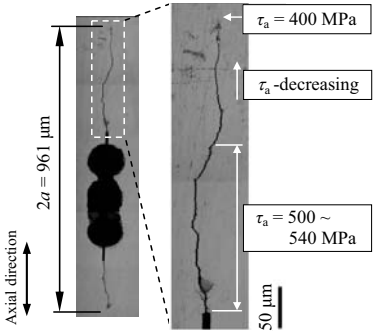

(a) Defect A (τ_a =540 MPa → 400 MPa, σ_m = –1200 MPa, N = 9.84×10^7)

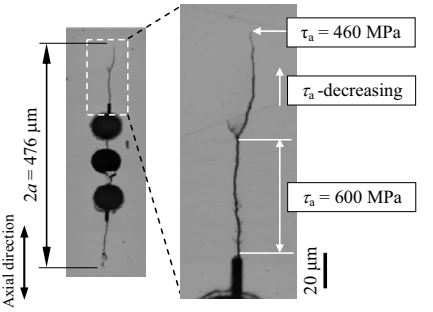

(b) Defect B (τ_a =600 MPa → 460 MPa, σ_m = –1200 MPa, N = 5.28×10^7)

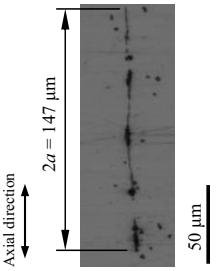

(d) Smooth specimen (τ_a = 600 MPa (constant), σ_m = –1000 MPa, N = 1×10^7)

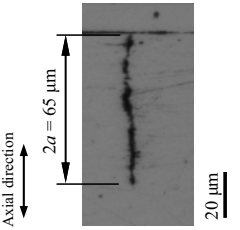

(d) Smooth specimen (τ_a = 600 MPa (constant), σ_m = –1000 MPa, N = 1×10^7)

Figure 6 Non-propagating cracks (Optical microscope)

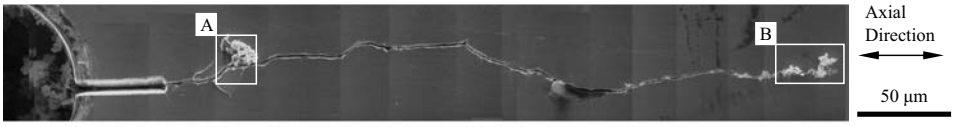

(a) Low magnification (SEM)

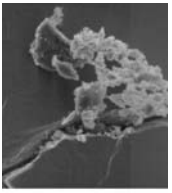

(b) Region A observed under high magnification

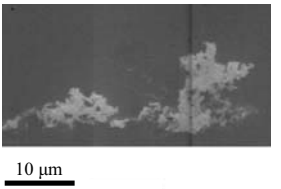

(b) Region B observed under high magnification

Figure 7 Abrasion powder occurring at crack faces of non-propagating crack during 10^6 cycles (N =9.74×10^7 ~ 9.84×10^7)

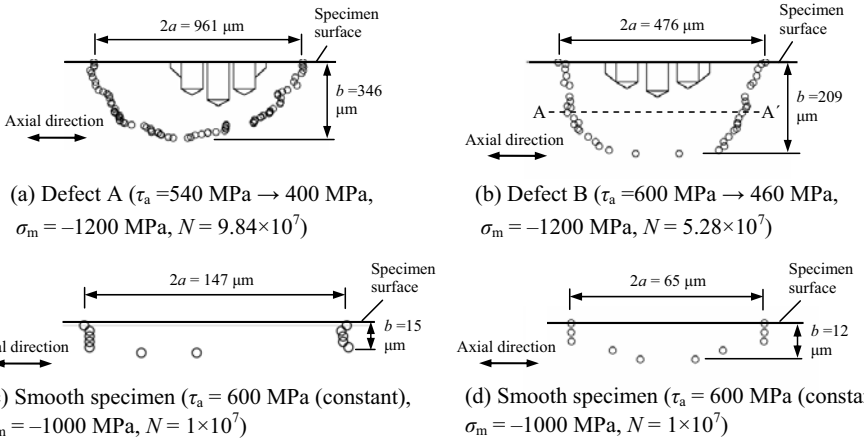

(a) Defect A (τ_a =540 MPa → 400 MPa, σ_m = –1200 MPa, $N = 9.84\times10^7$)

(b) Defect B (τ_a =600 MPa → 460 MPa, σ_m = –1200 MPa, $N = 5.28\times10^7$)

(c) Smooth specimen (τ_a = 600 MPa (constant), σ_m = –1000 MPa, $N = 1\times10^7$)

(d) Smooth specimen (τ_a = 600 MPa (constant), σ_m = –1000 MPa, $N = 1\times10^7$)

Figure 8 Shape and dimensions of non-propagating crack obtained by successive polishing

Table 1 lists the test conditions, the dimensions of non-propagating cracks and the threshold values. In the τ_a-constant test using smooth specimens with τ_a of 600 MPa, the values of ΔK_{II} and ΔK_{III} for non-propagating cracks do not necessarily mean the crack-growth threshold because the cracks might be able to stop propagating even at a slightly higher stress amplitude. Hence, such values were shown in parenthesis as the near-threshold values. Figure 9 shows the threshold values as a function of crack size. ΔK_{IIth} was plotted for the half crack length a, and ΔK_{IIIth} for the crack depth b, respectively. The threshold values decreased with a decrease in crack size where a or b is less than 1 mm. It is noted that in the τ_a-constant tests using smooth specimens, the aspect ratio b/a of the non-propagating cracks was strongly influenced by the shape of the elongated inclusions, i.e. it ranged from 0.2 to 0.4. The relatively shallow crack shape implied that the crack-growth threshold was mainly determined by the growth into the surface rather than along the surface. For this reason, the stress intensity factor ranges for such shallow cracks were estimated only for mode III propagation.

The difference between ΔK_{IIth} and ΔK_{IIIth} was not large when they were compared at equivalent crack sizes. Murakami *et al.* have suggested that the mechanism of mode III crack-growth is essentially the same as the mechanism of mode II crack-growth [10]. They concluded that the crack-growth resistance both in mode II and mode III is the same, i.e. $\Delta K_{IIth} = \Delta K_{IIIth}$ [11]. The results in the present study seem to support the hypothesis.

Although the threshold data obtained in the present study is considered a crack-growth resistance free from the contribution of compressive stress normal to crack face, the resistance can be influenced by crack-face friction. In order to evaluate the failure problem, the effect of friction must be further quantified.

Crack Initiation	Stress control	$\tau_{a\ start}$ [MPa]	$\tau_{a\ non\text{-}propagating}$ [MPa]	σ_m [MPa]	$2a$ [μm]	b [μm]	b/a	ΔK_{IIth} [MPa·m$^{0.5}$]	ΔK_{IIIth} [MPa·m$^{0.5}$]
Defect A	τ_a -decreasing	540	400	−1200	961	346	0.72	20.3	16.7
Defect B	τ_a -decreasing	600	460	−1200	476	209	0.88	17.9	13.4
Inclusion	τ_a -constant	600	600	−1000	172	36	0.42	—	(10.1)
Inclusion	τ_a -constant	600	600	−1000	147	15	0.20	—	(7.3)
Inclusion	τ_a -constant	600	600	−1000	65	12	0.37	—	(6.0)

Table1 Test conditions, dimensions of non-propagating cracks and threshold stress intensity factor ranges

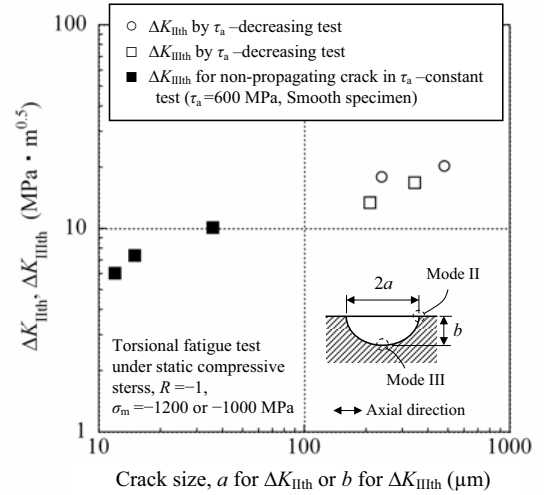

Figure 9 Relationship between crack sizes and crack-growth thresholds

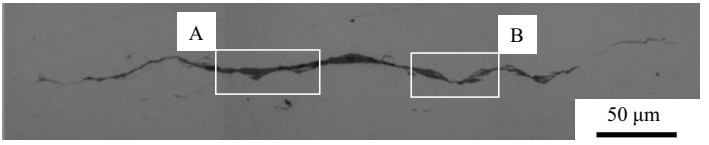

(a) Shear-mode fatigue crack at A−A' in Fig. 8 (b)

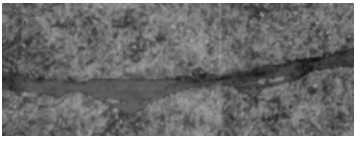

(b) Region A (Nital etched)

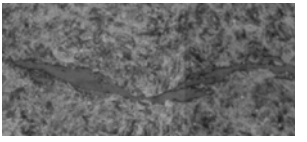

(c) Region B (Nital etched)

Figure 10 Microstructural change along shear-mode fatigue crack

Microstructural change along shear-mode crack. Figure 10 shows an etched microstructure at the section A-A′ of the crack shown in Fig. 8 (b). A gray band was observed along shear mode cracks. Such microstructural change is a typical characteristic of shear-mode fatigue crack-growth, and has been reported not only in bearing steels but also in a rail steel [4] and a medium carbon steel [12]. The gray bands were seldom observed in the vicinity of crack front, but were extensively observed at the central part of crack. For this reason, it was assumed that the microstructural change was caused by rubbing of crack faces during crack-growth.

Summary

Semi-elliptical shear-mode fatigue cracks were formed in the axial direction of round specimens of SAE52100 bearing steel by fully-reversed cyclic torsion tests under a static axial compressive stress. Threshold stresses for shear-mode crack-growth were obtained for various crack sizes less than 1 mm. The following conclusions were obtained.

(1) Threshold stress intensity factor ranges, ΔK_{IIth} and ΔK_{IIIth}, decreased with a decrease in crack size.

(2) The difference between ΔK_{IIth} and ΔK_{IIIth} was not large when they were compared at equivalent crack sizes.
(3) A microstructural change was caused by rubbing of crack faces during crack-growth.

Acknowledgement

This work was supported by funds from the Electro Mechanic Technology Advancing Foundation (EMTAF) and the Central Research Institute of Fukuoka University (No. 081501).

References

[1] Y. Murakami, *Transactions of the Japan Society of Mechanical Engineers*, Series A, Vol. 59 (1993), pp. 283-290

[2] S. Beretta, M. Boniardi, M. Carboni and H. Desimone, *Engineering Failure Analysis*, Vol. 12 (2005), pp. 157-165

[3] A. Otsuka, Y. Fujii and K. Maeda, *FFEMS*, Vol. 27 (2004), pp. 203-212

[4] Y. Murakami, T. Fukuhara and S. Hamada, *Journal of the Society of Materials Science, Japan*, Vol. 51 (2002), pp. 918-925

[5] M. Selecká and A. Šalak, *Wear*, Vol. 236 (1999), pp. 47-54

[6] Y. Murakami and H. Natsume, *JSME International Journal*, Series A, Vol. 45 (2002), pp. 161-169

[7] L.P. Pook, *Engineering Fracture Mechanics*, Vol. 48 (1994), pp. 367-378

[8] Z.P. Bažant and L.F. Estenssoro, *Int. J. Solids and Structures*, Vol. 15 (1979), pp. 405-426

[9] M.K. Kassir and G.C. Sih, *Journal of Applied Mechanics*, Vol. 33 (1966), pp. 601-611

[10] Y. Murakami, K. Takahashi and R. Kusumoto, *Fatigue Fract. Engng Mater. Struct.*, Vol. 26 (2003), pp.523-531

[11] Y. Murakami, Y. Fukushima, K. Toyama and S. Matsuoka, *Engineering Fracture Mechanics*, Vol. 75 (2007), pp. 306-318.

[12] K. Toyama, Y. Fukushima and Y. Murakami, *Journal of the Society of Materials Science, Japan*, Vol. 55 (2006), pp. 719-725